MODELLING OF A MICROGRID IN A PUBLIC BUILDING

Andy Nicolas Lerens
lerensandy@hotmail.com

Instituto Superior Técnico, Universidade de Lisboa, Portugal

January 2021

Abstract

The need to create sustainable, efficient and affordable energy is changing the way power systems operate and innovative solutions are being developed. Microgrids are one of this solutions and the work the conducted for this thesis serves towards the integration of this technology for the creation or retrofit of Near Zero Energy Buildings. The photovoltaic, energy storage system and inverters of an existing microgrid are modelled in Simulink, allowing for the evaluation of the viability and performance for the integration of this type of renewable energy resources but also to understand the interfacing elements between the generation and the load.

Key-words: energy; microgrid; sustainable; Renewable; Energy Storage System; Simulink; performance; photovoltaic.

1. Introduction

Energy is one of the principal pillars that sustain our economic and social development and its importance is relevant at all scales. From the statistics available in the International Energy Agency (IEA), the share of energy consumed in the transportation of goods and people in Portugal, represented 35% of the total final consumption in 2017, 28% for the industry, and 27% for residential, commercial and public services. Policies to reduce the carbon emissions, are driving the push for the integration and development of renewable energies to power the national grid, averting the use of fossil fuels plants and more carbon intensive alternatives. It is in this matter that microgrids can contribute to improving and acting upon the power grid interconnection and the inclusion of a bigger share of renewable energies in the power grid. Microgrids are the combination of various micro sources with rated power typically inferior to 100 kW and their interaction with the local load (power and heat). Microgrids operate connected with the conventional national power grid (supply and consumption) but can also function disconnected in islanded mode, autonomously. Generally, the Distributed Generation (DG) sources integrated in the microgrids consist of Renewable Energy Sources (RES), such as micro turbines, photovoltaic panels and Fuel Cells [1]. The developed model for the microgrid is based on a Microgrid currently operating in the grounds of the Laboratório Nacional de Energia e Geologia and is part of an international project called IMPROVEMENT focused on the retrofit of existing building into Near-Zero Energy Buildings (NZEB) with usage of microgrids armed with combined heat and power (CHP), RES and energy storage systems (ESS). Other objectives of the project include developing control and management systems to guarantee energy efficiency and power quality. The main features of microgrids that make them attractive include their ability to improve grid performance, be it in case of the utility grid failures or to complement existing power generation through integration of control systems, increase renewable energy penetration or energy management tools.

2. Literature Review

Microgrids can be classified by the type of power supplied in the distribution network or by the type of implementation. By type of implementation

Facility microgrids, utility microgrids and remote microgrids [2], and by bus distribution AC or DC.

An important property of microgrids are their ability to operate disconnected of the grid, mostly known as islanded mode of operation. Islanded mode of operation is the ability of a microgrid to disconnect from the utility grid at the point of common coupling (PCC). The consumers load is instead shifted to the microgrid DG and Energy storage system (when present), the distribution utility loses control of the supply, ceasing to guarantee power quality and stability. There are many reasons for a microgrid to transition to islanded mode some of these are economic purposes, reliability instances and/or to supply power in remote locations where the utility-grid is insufficient. Other arguments supportive for the implementation of microgrids are the grid performance support increasing the system reliability, resilience and power quality (PQ) [3].

[4] studies the economics and reliability of microgrid energy management systems compared the average service availability index (ASAI), system average interruption frequency index (SAIFI) and system average interruption duration index (SAIDI) for two different reliability simulations. The difference between the simulations is the inclusion of DERs. Resulting in, table 1, better ASAI, SAIFI and SAIDI performances for the grid with DERs. The paper authors suggest that the improved performance is due to the ability of islanding of the microgrid when the main grid fails.

SYSTEM RELIABILITY INDEX	WITHOUT DER	WITH DER
SAIFI (1/YR)	0.4893	0.3954
SAIDI (HR/YR)	4.486	3.961
ASAI	0.99931	0.99959

Table 1 - Reliability simulation for a grid with and without DERs [1]

[5] defines resiliency as the capability of power systems to sustain power in unlikely and high impact incidents, ensuring the least amount of disruption in the supply of electricity, enabling quick recovery and restoration of the normal steady state of operation. The implied incidents can take various forms, natural disasters, cyber-security attacks, military interventions, etc. Hence the motivation for the integration of resiliency microgrids in strategic locations that are susceptible to this range of conditions. In [6] a PQ analysis is performed for a microgrid located in Newcastle at the CSIRO. The main PQ issues are identified as, frequency and voltage variations, unbalanced voltages, current and voltages total harmonic distortion (THD). The paper suggests that future research for PQ improvements may pass through the integration of ESS for PQ compensation and optimum control and strategies.

3. Data and Methodology

The microgrid thermal generation and recuperation system comes from solar thermal collectors as the main source and three hybrid Photovoltaic panels (PV/T) with an heat exchanger to recuperate heat from the solar cells (design from LNEG). Similar to a general PV panel except that a heat exchanger system is placed in the back plate to extract heat from the solar modules to a working fluid, improving solar cell efficiency and pre-heating a domestic hot water (DHW) tank.

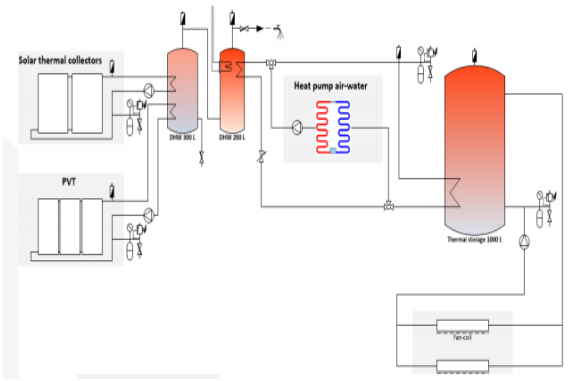

Figure 1 - LNEG's thermal system pilot plant

The electrical generation of the plant, shown in Figure 2, comes from a PV array with rated power of 4,05 kW, the previously mentioned PV/T panels rated for 0,69 kW , two Training PV panels in parallel rated for 0,56 kW and a small wind turbine rated for 2,5 kW connected to a permanent magnet synchronous generator (PMSG). The DER output generation is in DC and is connected to a 230/400 V AC bus, interfaced individually by inverters.

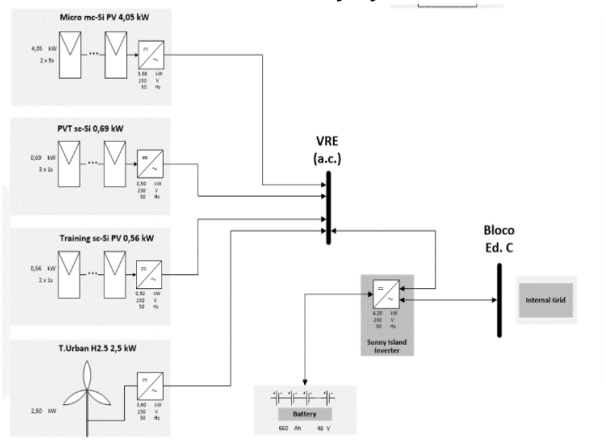

Figure 2 - LNEG's electrical system pilot plant

The electrical system of the microgrid is implemented in Matlab/Simulink and the following assumptions are made:

The mode of operation for the simulation will be in grid-tied mode, meaning that the inverters inter-connecting the Power generation and the internal grid of the building will take the grids reference for synchronization and control;
The loads of the microgrid are the heating pump, small appliances, and lighting, following a certain profile for the consumption;
The loads are assumed to only require active power;
Whenever the power generated is superior to load consumption, the battery will charge. And whenever the load is greater than the power generated the battery will discharge, to decrease the power drawn from the grid.

3.1 Photovoltaic System Modelling

The equivalent circuit of the general model of the PV Cell, figure 7, consists of a photo current I_L, a diode, a parallel resistor to represent leakage current and a series resistor to represent the internal resistance to the current flow [7]. The voltage-current characteristic equation of a solar cell is given as

$$\boldsymbol{I = I_L - I_S\left[exp\left(\frac{q(V+IR_S)}{kT_CA}\right) - 1\right] - \frac{(V+IR_S)}{R_{SH}}} \quad (1)$$

Where I_S is the cell saturation of dark current, q ($= 1.6 \times 10^{-19}\ C$) is the electron charge, k ($= 1.38 \times 10^{-23}\ J/K$) Boltzmann's constant, T_C is the cell temperature, A is an ideal factor, R_{SH} is a shunt resistance, and R_S is the series resistance. Some models consider $R_{SH} = \infty$ and $R_S = 0$ for additional simplification, assuming there is no current leakage or current flow resistance in series. The photocurrent mainly depends on the solar insolation and cell temperature which can be expressed as

$$\boldsymbol{I_L = [I_{SC} + K_I(T_C - T_{Ref})]\lambda} \quad (2)$$

With I_{SC} being the cell short-circuit current at 25 °C and irradiance 1000 W/m^2, K_I being the cell short-circuit current temperature coefficient, T_{Ref} is the cell reference temperature, and λ is the solar insolation in kW/m^2.

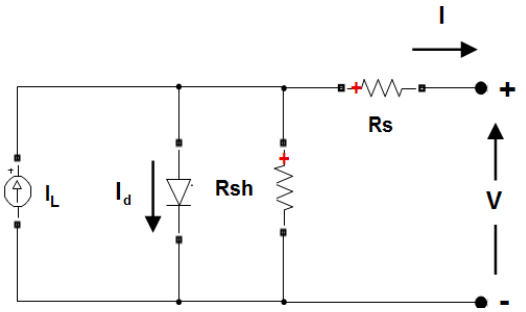

Figure 3 - Equivalent Circuit of PV Cell

The cell saturation current, I_S, is obtained in the following way

$$\boldsymbol{I_S = I_{RS}\left(\frac{T_C}{T_{Ref}}\right)^3 \exp\left[\frac{qE_G\left(\frac{1}{T_{Ref}} - \frac{1}{T_C}\right)}{kA}\right]} \quad (3)$$

Where I_{RS} represents the cell reverse saturation current at a reference temperature and solar radiation, E_G is the band-gap energy of the semiconductor in the cell, A is the ideality factor which is dependent on the type of semiconductor employed.
The typical power generation of PV cell is roughly 2 W at 0.5 V, requiring multiple cells connected in series-parallel to achieve a reasonable current and voltage rating. This configuration is called a PV module, the circuitry is then encased and protected in the PV panel. A PV array is a cluster of PV modules connected in series for appropriate Voltage and in parallel to increase current.

$$\boldsymbol{I = NpI_L - NpI_S\left[exp\left(\frac{q\left(\frac{V}{Ns} + \frac{IR_S}{Np}\right)}{kT_CA}\right) - 1\right] - \frac{\left(\frac{NpV}{Ns} + IR_S\right)}{R_{SH}}} \quad (4)$$

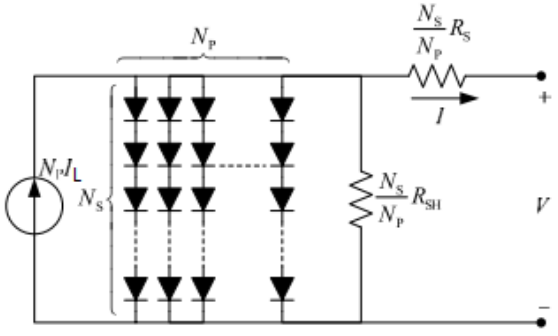

Figure 4 - Equivalent Circuit of PV Array

The properties of the PV module implemented in the 4 kW PV Array of the Microgrid are displayed in Table 2.

PV Module	LDK 225P-20

Nominal output (Pmax)	225 *W*
Voltage at Pmax (Vmp)	29.9 *V*
Current at Pmax (Imp)	7.35 *A*
Open Circuit Voltage (Voc)	36.7 *V*
Short Circuit Current [Isc]	8.24 *A*
Cell efficiency	15.89
Module Efficiency	13.79

Table 2 - Electric characteristics of the 4 kW PV Array

For the characterization of the photovoltaic Thermal (PV/T) collector used in the microgrid, very little information has been given. In this work the system will be interpreted as the fusion of the functions of a flat plate solar (thermal) collector and of a photovoltaic panel. The flat plate collector will remove the excess heat providing from the solar cells and transfer it to a working fluid. However, since the focus of the study is to determine the power generation, and not necessarily the heat transfer or the saving from pre-heating the DHW tank, the PV/T will be approximated to a simple PV Array of 690W composed of one string of three 230W rated power panels. The small 560 W PV array is composed of two 280 W rated power.

The optimum performance point can be identified as the one producing the most power. The point is called Maximum Power Point (MPP), the PV array by itself cannot regulate to operate at this point. For this reason, Maximum power point tracking (MPPT) algorithms can be developed to achieve MPP. The algorithm used to draw the maximum power from the PV source, in this study, is called Perturb and Observe. In this method, the MPP is reached by calculating the PV output power and the change in power by sampling the PV array voltage and current. The algorithm increments or decrements the voltage, if the perturbation leads to an increase in power, then the algorithm follows this path, if not, the algorithm perturbs in the opposite direction. A flowchart of the algorithm is presented in

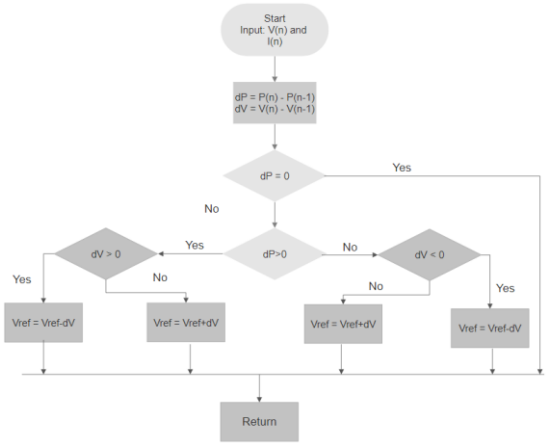

Figure 5 - Perturb and Observe algorithm flow chart

3.2 Energy Storage System

The Battery type used in the microgrid is of the Lithium-Ion (Li-Ion) type. One of the advantages of using a Li-Ion type of battery, is that the cells that form the battery operate at a voltage three times higher than usual NiMH or NiCd batteries, at 3.7 V. For this reason, Li-Ion batteries present a higher energy density (*Wh/Kg*). The typical discharge characteristics of a battery can be found in Figure 6. Three sections of the curve are outlined. The exponential voltage drops when the battery starts discharging after being fully charged, is represented in the first section, the width of the zone is strongly related to the type of battery used. The following section, and the widest is the charge that can be extracted from the battery until the voltage drops below the nominal voltage of the battery. After the voltage drops below the nominal value, it starts to drop rapidly until no more power is extractable

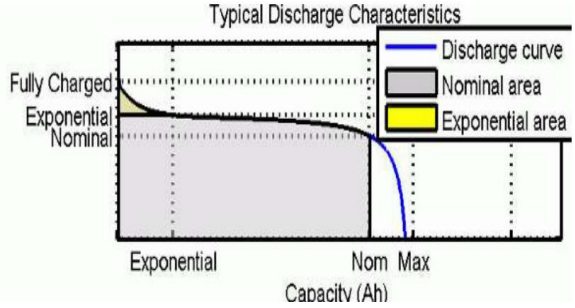

Figure 6 - Typical Discharge Characteristic of a Battery

The model of the battery used for the simulation is based on the Simscape Power Systems Library battery, the battery block implements a generic dynamic model that represents most commonly found types of rechargeable batteries [8].

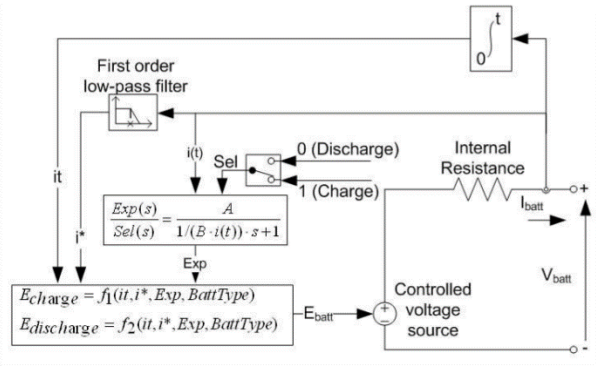

Figure 7 - Equivalent Circuit of Battery Simscape block

The parameters and variables of the model are:

- Ebatt Nonlinear Voltage (V)
- E0 Constant Voltage (V)
- Exp(s) Exponential Zone Dynamics (V)
- Sel(s) Battery mode, 0 for discharge 1 for charge
- K Polarization constant (Ah-1) or Polarization resistance (Ω)
- i* Low frequency current dynamics (A)
- i Battery Current (A)
- it Extracted Capacity (Ah)
- Q Maximum Battery Capacity (Ah)
- A Exponential Voltage (V)
- B Exponential Capacity (Ah-1)

The discharge model for the Li-Ion Battery $i^* > 0$ is

$$f_1(it, i, i^*) = E_0 - K.\frac{Q}{Q - it}.i^* - K.\frac{Q}{Q - it}.it + A.exp(-B.it) \quad (5)$$

And the charge model is

$$f_2(it, i, i^*) = E_0 - K.\frac{Q}{it - 0.1.Q}.i^* - K.\frac{Q}{Q - it}.it - A.exp(-B.it) \quad (6)$$

4. Implementation

4.2 Photovoltaic Systems

Each generator of the microgrid is modelled and simulated separately before the microgrid assembly, to ensure that the models are robust enough to give decent results when finally tested. The model of the 4 kW PV array, along with the two-stage inverter is presented in Figure 8. The PV Array input is the global irradiance (Ir) over the surface of the panel and the temperature of the cell (Tcell), the PV Array terminals are connected to a DC/DC boost converter to step up the voltage of the array to constant 600V, whilst maintaining optimum generation. The boost converter is then connected to the DC/AC Inverter converting the 600 V DC to the 230/400 V (phase to ground/phase to phase) AC Bus and Grid. The LCL filter is used to reduce the harmonics and flickers generated by the converters, for smoother sinusoidal waves at the output.

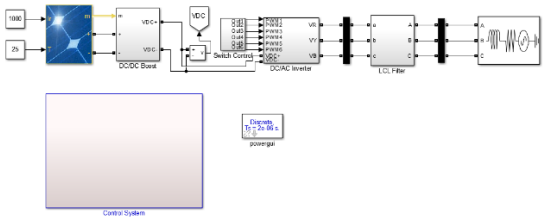

Figure 8 - Grid connected model of PV Array

Many studies that investigate the PV array modelling use the ambient temperature to represent the cell temperature, however this assumption is not representative of every situation, the study [9] calculates the cell temperature, with the Equation 7, as a function of the air temperature and irradiance variation.

$$T_{cell} = 1.14(T - T_{STC}) + 0.0175(G - 300) + 30 \quad (7)$$

The proposed MPPT algorithm, is integrated through a DC/DC Boost converter. It generates a signal that is fed to the PWM generator, creating a duty signal that will control the circuit's switch. The pulsation on the switch is responsible for drawing the MPP from the PV array, increasing or decreasing the voltage.

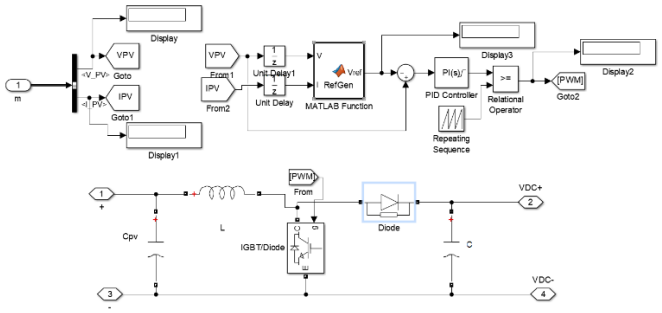

Figure 9 - Modeled 600 V DC/DC Boost Converter

Each of the photovoltaic sources used the modeled structure to connect to the AC bus. The parameters of modeled DC/DC boost converter are presented in table 12 and their calculation use [10] as reference.

	Vin	Vdc	Switch freq.	L	C	Cpv

4 kW PV Array	230 V	600 V	5000 Hz	8 mH	1500 µF	2000 µF
690 W PV Array	75 V	600 V	5000 Hz	156 mH	186 µF	1000 µF
560W PV Array	50 V	600 V	5000 Hz	127 mH	229 µF	1000 µF

Table 3 - DC/DC Boost Converter Parameters

The three phase current Iabc is sampled at the inverter output and transformed into dq0 reference frame using Clarke and Park transformation, Id current corresponds to the active current and Iq corresponds to the reactive current. The P and Q powers can be calculated such that

(8)

$$P = \frac{3}{2} u_d \, i_d$$

$$Q = -\frac{3}{2} u_d \, i_q \quad (9)$$

Where u_d and u_q are the respective dq axis components of the three-phase grid voltage, by controlling i_d and i_q, we are controlling the active and reactive power of the system.

The respective currents are then compared with their reference value, generating an error that is fed to the PI controller. The q axis current is forced to be 0 due to the considered simplified scenario where only active power is fed to the grid. The resulting signals are then processed in the current controller composed of individual PI controllers for each of the two signals, and generated modulation signals for the voltage in the d and q axis. The voltage drop through the filter inductor is compensated and added with the respective dq axis voltages and fed to the dq to abc block to generate the voltage reference for the PWM generator, the control diagram is shown in Figure 10. The control algorithm follows the methodologie of [11][12][13] For a Sine Wave PWM modulation scheme, the relation between modulation index and the inverter voltage is given by:

$$v_d = m_d \frac{V_{DC}}{2} \quad (10)$$

$$v_q = m_q \frac{V_{DC}}{2} \quad (11)$$

Decoupling the previous dynamic

$$m_d = \frac{2}{V_{DC}} [v_d - (\omega L i_q) + u_d] \quad (12)$$

$$m_q = \frac{2}{V_{DC}} [v_q + (\omega L i_d) + u_q] \quad (13)$$

Where i_{dref} and i_{qref} are the d-q axis reference currents, i_d and i_q are the respective dq axis components of the three-phase inverter output, $\omega L i_q$ represents the voltage drop across the filter inductor, with $\omega = 2\pi f_{grid}$ and L the value of the filter inductor.

If we define v_{td} and v_{tq} as the d-axis and q-axis components of the inverter output terminal, then the control equations can be written as

$$v_{td} = (K_p + K_i/s)(i_{dref} - i_d) - (\omega L i_q) + u_d \quad (14)$$

$$v_{tq} = \left(K_p + \frac{K_i}{s}\right)(i_{qref} - q) + (\omega L i_d) + u_q \quad (15)$$

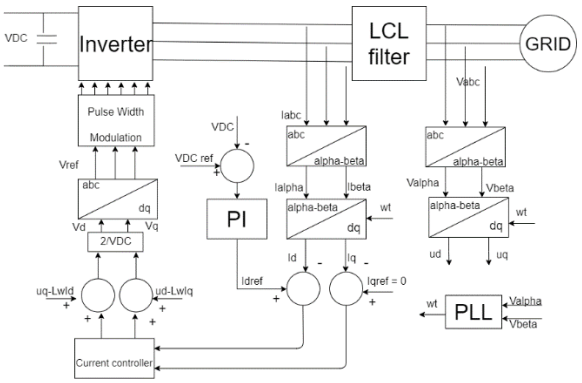

Figure 10 - Two Stage Inverter decoupled control diagram

System Parameters	
Three-phase Grid Voltage, *Vg*	230/400 V AC
Grid frequency, f_{grid}	50 Hz
Switching Frequency of inverter, fsw	5 kHz
DC voltage at Inverter Input	600 V

Table 4 – System Parameters

4.3 Energy Storage System

The battery model used for this simulation is a Li-Ion Battery with 48V Nominal Voltage, 660 Ah rated capacity. The Battery Model Parameters are calculated with Simscape Power System battery, based on the nominal properties. The calculated discharge properties are presented in Table 5 however the properties are assumed identical for charging.

Maximum Capacity (Ah)	660
Cut-Off Voltage (V)	36
Fully Charged voltage (V)	55.8714
Nominal Discharge Current (A)	286.9565
Internal Resistance (Ω)	0.00072727
Capacity at Nominal Voltage (Ah)	596.8696
Exponential Zone Voltage (V)	51.8585
Exponential Zone Capacity (Ah)	32.4261

Table 5 - 48V 660 Ah Battery Discharge Properties

A Bi-directional Buck/Boost converter connected to battery is necessary for the microgrid mode of operation. The circuit must be able to either buck the current to a reasonable voltage for the battery so it can charge, or boost the current discharged by the battery to the AC Bus for it to meet the requirements so that the inverter is able to output the power with appropriate voltage. The DC voltage is maintained constant at the terminals of the inverter, at 600 V. The approach, based on the methodologies of [14] controls the direction of the flow through a reference current generated, considering the conditions and power balance of the microgrid.

4.3 Microgrid

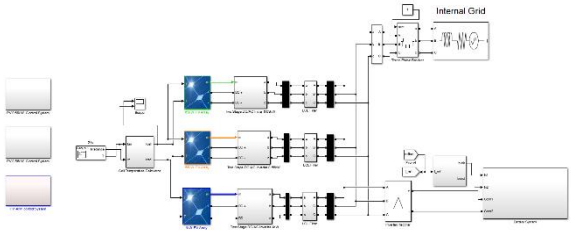

Figure 11 - Microgrid Model

The modelled layout of the microgrid is presented in Figure 11 the three different PV sources and their respective two stage inverters, interfaced by an LCL filter, connected to the grid. The internal grid of the building is represented by the three phase source, which allows to specify the phase-to-phase voltage, frequency and the internal impedance. The phase-to-phase voltage and frequency are chosen to be Vpp = 400V and 50Hz as it represents the conditions for the energy distribution in Portugal.

5. Results

5.1 Testing of the Microgrid

The evaluation of the performance of MPPT algorithm is done through measuring the voltage and current generated by the PV with MPPT and obtain the power curve. For comparison an ideal curve is generated based on the maximum power obtained at Standard Testing Conditions (STC). In Figure 12, the black dotted line represents the theoretical maximum power available for the 4 kW PV Array and pink line is the generated power. The red line represents the efficiency of the algorithm, obtaining a close to 1 value.

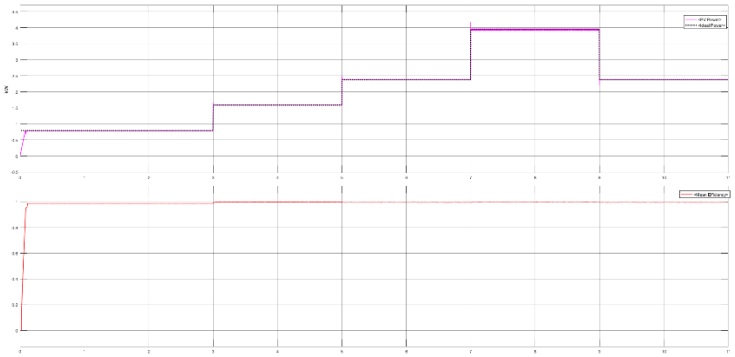

Figure 12 - MPPT algorithm performance

Another test is performed at STC conditions to evaluate the current output and THD. The voltage and Current fed to the AC Bus by the photovoltaics generators is seen in Figure 13 and the THD of the current is shown in Figure 14.

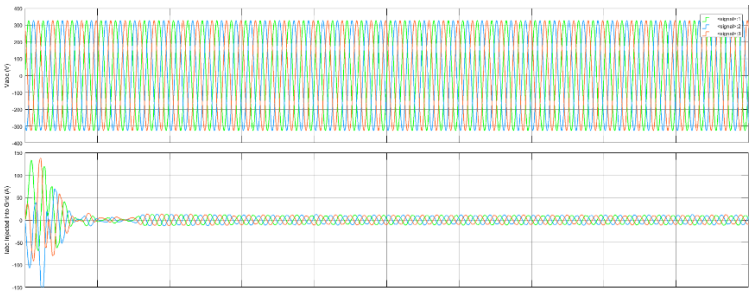

Figure 13 - Vabc and Iabc measured in Microgrid AC Bus

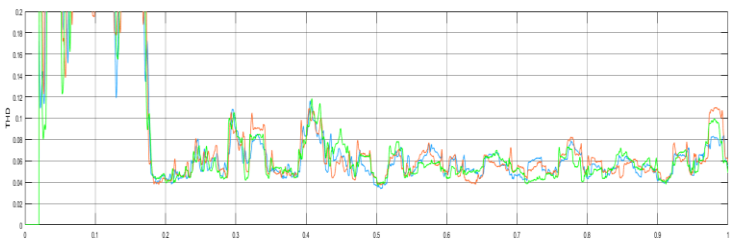

Figure 14 – Total Harmonic Distortion for the AC Bus Current

The high THD is caused flickers in the control signal of the direct current, and can be further reduced with proper tuning.

5.2 Daily Simulation

A daily simulation is set up by inputting the temperature and irradiance data for a summer day. The load profile follows a typical working hours curve and in presented in Figure 15.

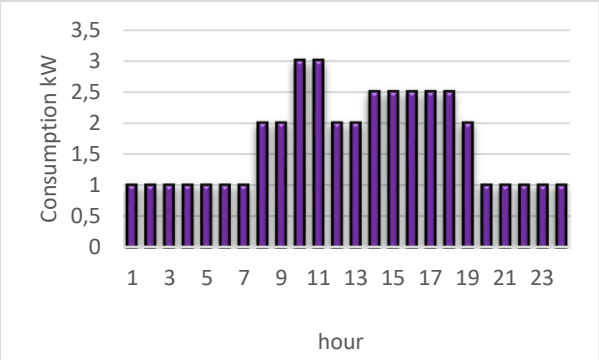

Figure 15 – Load profile for the simulation

The obtained curves for the simulation are presented in Figure 16, the green curve being the sum of all the power generated by the photovoltaic arrays peaking at 4600 W around mid-day.

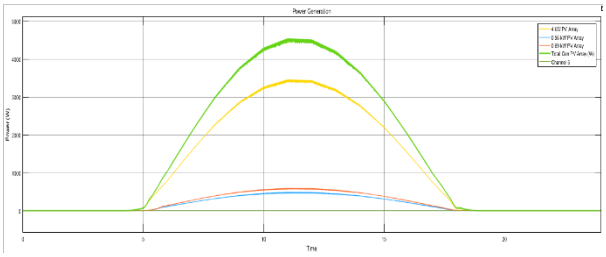

Figure 16 – Photovoltaic Power Generation

The power balance between the generation and the load and a curve is obtained. Whenever the values of the curve are greater than 0 the generation is greater than the load, otherwise the load is greater than the generation and the battery must discharge into the AC bus to feed the Load.

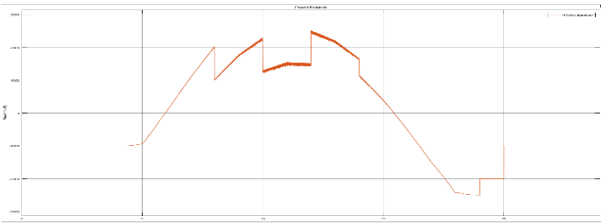

Figure 17 – Power balance of the Microgrid

The State of Charge (SOC) of the battery and its battery current are shown in Figure 18.

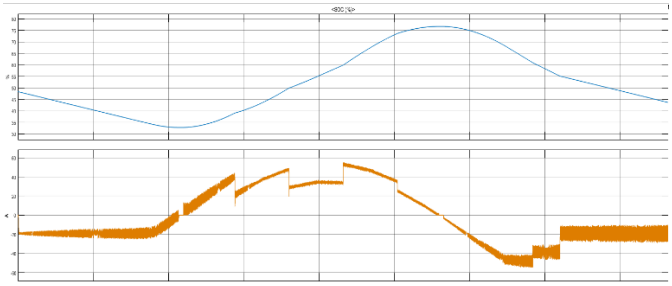

Figure 18 – State of Charge of the Battery for the daily simulation and battery current terminals.

5.3 Annual Simulation Results

The dataset to perform the annual simulation is comprised of 8760 values for the air temperature and irradiance in Lisbon, each corresponding to the average value for the hour of the year of 2016

The obtained mean photovoltaic generation for the simulation, is presented in Table 1.

Source	Annual Mean Power (kW)	Mean annual Energy Generated (kWh)
PV1 – 4kW Rated	0.689	6035.6
PV2 – 0.69 kW Rated	0.101	884.8
PV3 – 0.56 kW Rated	0.088	770.9
Total Generation	0.878	7690.8
Load	2.09	18308.4
Power Balance	-	-10617.6

Table 1 – Mean Annual Generation and Load

6. Conclusion

The work performed in the thesis allowed to model three of the power generators presented in the microgrid and design their converting control system.

Further work includes creating a model for the WECS and integrate it with the electrical system and thermal system, adapt the model to be able to detect fault conditions and be able to switch to Island Mode within the power quality conditions. Create an intelligent microgrid management system with the capability to determine whenever the excess power should be sold to the grid or be stored in ESS, through economic analysis and predictive control.

REFERENCES

[1] R. H. Lasseter, "MicroGrids: A Conceptual Solution," *2002 IEEE Power Eng. Soc. Winter Meet. Conf. Proc. (Cat. No.02CH37309)*, vol. 1, pp. 305–308, 2002, doi: 10.1109/PESW.2002.985003.

[2] E. Hossain, E. Kabalci, R. Bayindir, and R. Perez, "Microgrid testbeds around the world: State of art," *Energy Convers. Manag.*, vol. 86, pp. 132–153, 2014, doi: 10.1016/j.enconman.2014.05.012.

[3] S. Parhizi, H. Lotfi, A. Khodaei, and S. Bahramirad, "State of the art in research on microgrids: A review," *IEEE Access*, vol. 3, pp. 890–925, 2015, doi: 10.1109/ACCESS.2015.2443119.

[4] H. Daneshi and H. Khorashadi-Zadeh, "Microgrid energy management system: A study of reliability and economic issues," *IEEE Power Energy Soc. Gen. Meet.*, pp. 1–5, 2012, doi: 10.1109/PESGM.2012.6344957.

[5] A. Khodaei, "Resiliency-oriented microgrid optimal scheduling," *IEEE Trans. Smart Grid*, vol. 5, no. 4, pp. 1584–1591, 2014, doi: 10.1109/TSG.2014.2311465

[6] A. Vinayagam, K. Swarna, S. Y. Khoo, and A. Stojcevski, "Power Quality Analysis in Microgrid: An Experimental Approach," *J. Power Energy Eng.*, vol. 04, no. 04, pp. 17–34, 2016, doi: 10.4236/jpee.2016.44003

[7] H. Tsai, C. Tu, and Y. Su, "Development of Generalized Photovoltaic Model Using MATLAB/SIMULINK," *Lect. Notes Eng. Comput. Sci.*, vol. 2173, no. 1, pp. 846–851, 2008.

[8] "Generic battery model - Simulink." https://www.mathworks.com/help/physmod/sps/powersys/ref/battery.html (accessed Dec. 12, 2020).

[9] R. Ayaz, I. Nakir, and M. Tanrioven, "An improved matlab-simulink model of pv module considering ambient conditions," *Int. J. Photoenergy*, vol. 2014, 2014, doi: 10.1155/2014/315893.

[10] B. Hauke, "Basic Calculation of a Boost Converter's Power Stage," *Texas Instruments, Appl. Rep. Novemb.*, no. November 2009, pp. 1–9, 2009, [Online].

[11] M. Lakshmi and S. Hemamalini, "Decoupled control of grid connected photovoltaic system using fractional order controller," *Ain Shams Eng. J.*, vol. 9, no. 4, pp. 927–937, 2018, doi: 10.1016/j.asej.2016.06.002.

[12] M. Lakshmi and S. Hemamalini, "Decoupled control of grid connected photovoltaic system using fractional order controller," *Ain Shams Eng. J.*, vol. 9, no. 4, pp. 927–937, 2018, doi: 10.1016/j.asej.2016.06.002.

[13] P. K. Khatua, V. K. Ramachandaramurthy, J. Y. Yong, and J. Pasupuleti, "Decoupled Control of Three Phase Grid Connected Solar PV System," *Int. J. Eng. Adv. Technol.*, vol. 9, no. 2, pp. 4218–4222, 2019, doi: 10.35940/ijeat.b4933.129219.

[14] M. Saleh, Y. Esa, Y. Mhandi, W. Brandauer, and A. Mohamed, "Design and implementation of CCNY DC microgrid testbed," *IEEE Ind. Appl. Soc. 52nd Annu. Meet. IAS 2016*, pp. 1–7, 2016, doi: 10.1109/IAS.2016.7731870.